

## A 3D columnar phase of stacked short DNA organized by coherent membrane undulations

Nathan F. Bouxsein, Cecilia Leal, Christopher S McAllister,  
Youli Li, Kai K Ewert, Charles E. Samuel, and Cyrus R Safinya

*Langmuir*, Just Accepted Manuscript • DOI: 10.1021/acs.langmuir.9b01726 • Publication Date (Web): 13 Aug 2019

Downloaded from pubs.acs.org on August 19, 2019

### Just Accepted

“Just Accepted” manuscripts have been peer-reviewed and accepted for publication. They are posted online prior to technical editing, formatting for publication and author proofing. The American Chemical Society provides “Just Accepted” as a service to the research community to expedite the dissemination of scientific material as soon as possible after acceptance. “Just Accepted” manuscripts appear in full in PDF format accompanied by an HTML abstract. “Just Accepted” manuscripts have been fully peer reviewed, but should not be considered the official version of record. They are citable by the Digital Object Identifier (DOI®). “Just Accepted” is an optional service offered to authors. Therefore, the “Just Accepted” Web site may not include all articles that will be published in the journal. After a manuscript is technically edited and formatted, it will be removed from the “Just Accepted” Web site and published as an ASAP article. Note that technical editing may introduce minor changes to the manuscript text and/or graphics which could affect content, and all legal disclaimers and ethical guidelines that apply to the journal pertain. ACS cannot be held responsible for errors or consequences arising from the use of information contained in these “Just Accepted” manuscripts.

# A 3D columnar phase of stacked short DNA organized by coherent membrane undulations

Nathan F. Bouxsein<sup>1</sup>, Cecília Leal<sup>2</sup>, Christopher S. McAllister<sup>3§</sup>, Youli Li<sup>4</sup>, Kai K. Ewert<sup>1</sup>, Charles E. Samuel<sup>3</sup>, and Cyrus R. Safinya<sup>1\*</sup>

<sup>1</sup> Materials Department, Physics Department, Molecular, Cellular, and Developmental Biology Department, University of California, Santa Barbara, California 93106, USA

<sup>2</sup> Department of Materials Science and Engineering, University of Illinois Urbana-Champaign, Urbana, IL 61801, USA

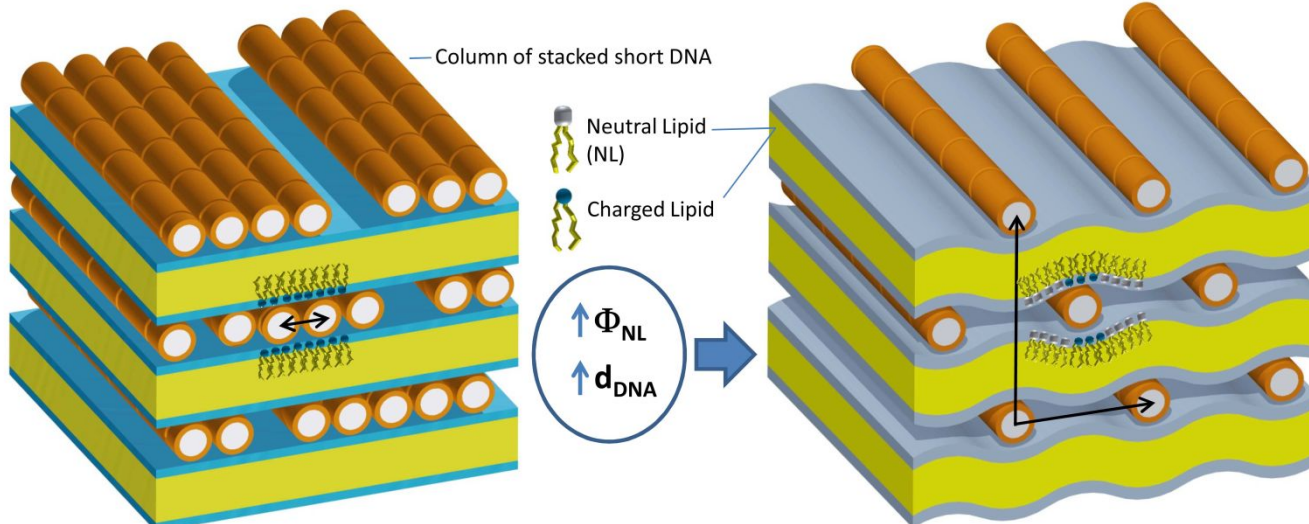
<sup>3</sup> Molecular, Cellular, and Developmental Biology Department, University of California, Santa Barbara, California 93106, USA

<sup>4</sup> Materials Research Laboratory, University of California, Santa Barbara, California 93106, USA

<sup>6</sup>Present Address: Genomics Institute of the Novartis Research Foundation, San Diego, CA 92121, USA

\*Corresponding author contact information: safinya@mrl.ucsb.edu

## GRAPHIC FOR TOC



## ABSTRACT

We report on the discovery of a new organized lipid-nucleic acid phase upon intercalation of blunt duplexes of short DNA (sDNA) within cationic multilayer fluid membranes. End-to-end interactions between sDNA leads to columnar stacks. At high membrane charge density, with the inter-sDNA column spacing ( $d_{sDNA}$ ) comparable but larger than the diameter of sDNA, a 2D columnar phase (i.e. a 2D smectic) is found similar to the phase in cationic liposome-DNA complexes with long lambda-phage

1 DNA. Remarkably, with increasing  $d_{sDNA}$  as the membrane charge density is lowered, a transition is  
2 observed to a 3D columnar phase of stacked sDNA. This occurs even though direct DNA-DNA  
3 electrostatic interactions across layers are screened by diffusing cationic lipids near the phosphate  
4 groups of sDNA. Softening of the membrane bending rigidity ( $\kappa$ ), which further promotes membrane  
5 undulations, significantly enhances the 3D columnar phase. These observations are consistent with a  
6 model by Schiessel and Aranda-Espinoza where local membrane undulations, due to  
7 electrostatically-induced membrane wrapping around sDNA columns, phase lock from layer-to-layer,  
8 thereby precipitating coherent “crystal-like” undulations coupled to sDNA columns with long-range  
9 position and orientation order. The finding that this new phase is stable at large  $d_{sDNA}$  and enhanced with  
10 decreasing  $\kappa$  is further supportive of the model where the elastic cost of membrane deformation per unit  
11 area around sDNA columns ( $\propto \kappa h^2/d_{sDNA}^4$ ,  $h^2$  = sum of square of amplitudes of the inner and outer  
12 monolayer undulations) is strongly reduced relative to the favorable electrostatic attractions of partially  
13 wrapped membrane around sDNA columns. The findings have broad implications in the design of  
14 membrane-mediated assembly of functional nanoparticles in 3D.

### 34 Key words

35 Stacked short-DNA, columnar phase, 3D membrane undulations, synchrotron SAXS

## 40 INTRODUCTION

41 Self-assembled complexes of cationic liposomes (CLs) and nucleic acids (NA) have been of  
42 significant interest to the field of nucleic acid nanomaterials. This, in part, is because of the ability to  
43 organize DNA and RNA in three-dimensional (3D) space in a variety of geometries with distinct lattice  
44 symmetries due to the electrostatic coupling of nucleic acids to charged membranes (1-18). Distinct  
45 CL-NA structures revealed by synchrotron x-ray diffraction include the lamellar  $L_{\alpha}^C$  with DNA  
46 sandwiched between cationic membranes (1,10); the inverted hexagonal  $H_{II}^C$  with DNA or stacked short  
47 DNA encapsulated within inverse lipid tubules (3,15); and the  $H_I^C$  structure, where cationic multivalent  
48

1 lipids with large positive spontaneous curvature lead to hexagonally arranged rod-like micelles  
2 surrounded with DNA chains forming a continuous substructure with honeycomb symmetry (11). For  
3 short double-stranded RNA, bicontinuous cubic phases, including the gyroid  $Q_{II}^{G, NA}$ , may be realized  
4 containing the RNA molecules on curved surfaces with negative Gaussian curvature (13,16-18). In  
5 addition to the scientific interest arising from the different structural arrangements of nucleic acids on  
6 membrane templates, CL-NA complexes are also of high biomedical interest because of their  
7 applications in delivery of therapeutic nucleic acids, both DNA (19-32) and short RNA  
8 (13,16-20,23,26,27,29-31,33-42) into cells. The high level of research interest in CL-NA complexes is  
9 complemented with more than 110 ongoing gene therapy trials worldwide using CL based carriers  
10 (vectors) (43,44).

11  
12  
13  
14  
15  
16  
17  
18  
19  
20  
21  
22  
23  
24 The precise nature of long DNA chains confined between cationic bilayer sheets in the lamellar  $L_\alpha^C$   
25 phase has been well elucidated through careful line-shape analysis of the structure factor obtained by  
26 synchrotron x-ray scattering. These analyses show that DNA chains form a finite-sized 1D lattice on the  
27 scale of the persistence length of DNA ( $\xi_p \approx 500 \text{ \AA}$  to  $1000 \text{ \AA}$ ) with weak cross bilayer correlations  
28 (45,46). Thus, DNA chains in each two-dimensional (2D) layer are nearly decoupled 2D smectics (or  
29 equivalently a 2D columnar phase) on length scales up to  $\approx \xi_p$ .  
30  
31

32 For long DNA, modeled as rigid rods confined between flat bilayer membranes, equilibrium theories  
33 have described a 3D columnar phase where DNA rods have long-range positional and orientational  
34 correlations across the bilayers (4,5,9). The models also predict a new phase of matter, which remains to  
35 be observed in experiments, referred to as a “sliding columnar” phase where DNA rods forming a 2D  
36 columnar phase lose positional correlations between bilayers but maintain 3D long-range (LR)  
37 orientational order. It is important to emphasize that in these models describing DNA arrangements on  
38 flat lipid bilayers, membrane undulations play no role in the equilibrium properties of the phases. Thus,  
39 long-range repulsive electrostatic forces between DNA rods in different layers stabilizes the 3D  
40 columnar phase.  
41  
42  
43  
44  
45  
46  
47  
48  
49  
50  
51  
52  
53  
54  
55  
56  
57  
58  
59  
60

1 In this paper, we combined cationic liposomes (CLs) consisting of mixtures of the cationic lipid  
2 1,2-dioleoyl-3-trimethylammonium-propane (DOTAP) and neutral lipid  
3 1,2-dioleoyl-sn-glycero-3-phosphocholine (DOPC) with blunt short DNA (sDNA) consisting of either  
4 11bp, 24bp or 48bp. Both lipids are in their chain-melted conformation forming fluid (i.e. liquid state)  
5 membranes in the temperature range studied (ambient room temperature to  $\approx 80$  °C). Synchrotron x-ray  
6 scattering experiments show that all three lengths of blunt sDNA form lamellar complexes with sDNA  
7 intercalated between the lipid bilayers. DNA-DNA correlations can be clearly elucidated from the  
8 scattering data revealing two highly organized arrangements of sDNA. These organization are only  
9 possible if sDNA rods stack end to end to form long columns (see Fig. 1A). This is consistent with a  
10 previous study that established blunt duplexes of sDNA in water preferentially stack end-to-end,  
11 forming sDNA columns to minimize exposure of the hydrophobic ends of the duplex to the aqueous  
12 environment (47,48). Finally, the analysis of short pieces of DNA with nonpairing overhangs adsorbed  
13 on 2D membranes has found that tuning of end-to-end stacking interactions, by altering number of the  
14 nonpairing overhangs, results in finite length stacks of sDNA (14).  
15  
16  
17  
18  
19  
20  
21  
22  
23  
24  
25  
26  
27  
28  
29  
30  
31  
32  
33  
34  
35  
36  
37  
38  
39  
40  
41  
42  
43  
44  
45  
46  
47  
48  
49  
50  
51  
52  
53  
54  
55  
56  
57  
58  
59  
60

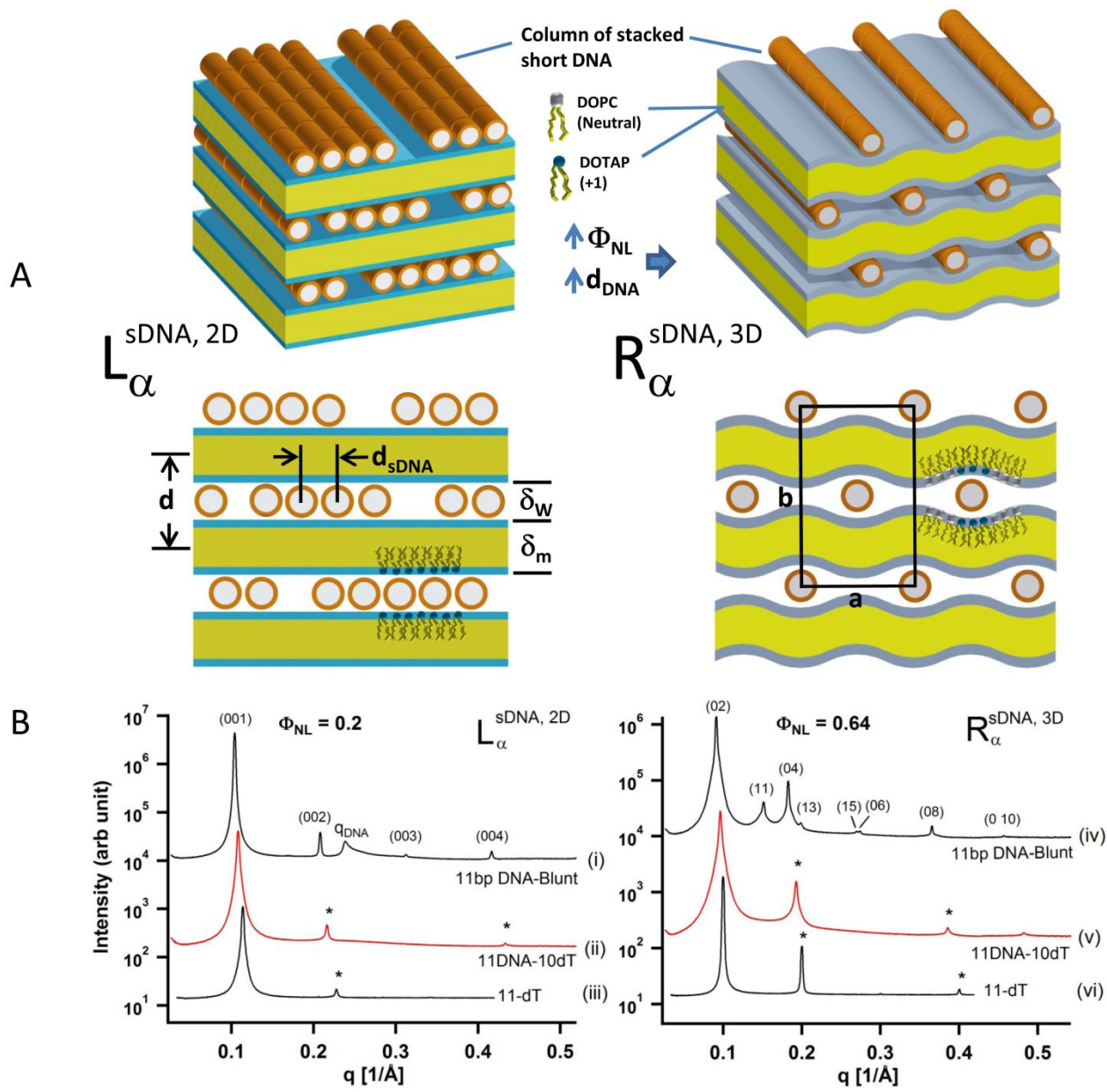


**Figure 1.** 2D ( $L_{\alpha}^{sDNA, 2D}$ ) and 3D columnar phases ( $R_{\alpha}^{sDNA, 3D}$ ) of stacked blunt short-DNA (sDNA) intercalated between fluid cationic lipid membranes (CL), revealed by synchrotron-based small angle x-ray scattering (SAXS). (A) LEFT: Graphic illustration of CL-sDNA complexes in the  $L_{\alpha}^{sDNA, 2D}$  phases. Formed at low mole fraction neutral lipid ( $\Phi_{NL}$ ) the stacked sDNA (depicted as short cylinders) sandwiched between cationic membranes form columns with a well defined DNA interaxial spacing in each layer, but without correlations from layer to layer. This phase is qualitatively similar to the previously observed 2D smectic like organization of long DNA in cationic liposome-DNA complexes (1,13,14). RIGHT: Graphic illustration of CL-sDNA complexes in the  $R_{\alpha}^{sDNA, 3D}$  phase, which forms after  $\Phi_{NL}$  is increased above a certain threshold ( $0.5 < \Phi_{NL} \leq 0.75$  for 11bp and 24bp sDNA, and  $0.52 < \Phi_{NL} \leq 0.75$  for 48bp sDNA). In this phase, the sDNA rods across the bilayers exhibit strong correlations, forming a centered rectangular lattice with long range order. The stacked

1 sDNA rods retain sliding degree of freedom along the helical axis. (B) (i) synchrotron x-ray scattering data of 11bp sDNA  
2 complexed with DOTAP/DOPC CLs for  $\Phi_{NL} = 0.2$  at the isoelectric point. The presence of a series of peaks resulting from  
3 the membrane stack and a highly asymmetric DNA 1D ordering peak is similar to what has been observed from CL-DNA  
4 complexes with long DNAs. The strong asymmetric lineshape is a direct indication of lack of the positional correlations of  
5 the 1D lattices across layers. This similarity to long CL-DNA data is evidence that the sDNA rods must be stacked  
6 end-to-end to form long columns. (ii) Diffraction data of 11DNA-10dT complexes at  $\Phi_{NL} = 0.2$ . The 11DNA-10dT has the  
7 same DNA core (11 bp, perfectly duplexed) but including 10 unpaired deoxythymidine nucleotides to each 3' end of the  
8 duplex. The introduction of dangling ends prevent end-to-end stacking and led to a very broad (barely visible) DNA  
9 correlation peak indicating that the DNA ordering is significantly hindered. (iii) Diffraction data from complexes made with  
10 a 11-base single-stranded homopolymer of deoxythymidine (11dT). There is no correlation peak from the 11dT ssDNA. (iv)  
11 Typical scattering profile of CL-sDNA complexes in the ordered  $R_{\alpha}^{sDNA,3D}$  phase for 11bp sDNA at  $\Phi_{NL} = 0.64$ . The sharp  
12 peaks can be indexed to a centered rectangular columnar structure with 2D lattice parameters  $a$  (=center-to-center spacing of  
13 stacked sDNA columns=45.9 Å at  $\Phi_{NL}=0.64$ ) and  $b$  (= 2\*interlayer spacing  $d = 138.8$  Å at  $\Phi_{NL} = 0.64$ ) as shown in Fig.1 A  
14 (RIGHT). (v, vi) Comparison diffraction data for CL-DNA complexes with 11DNA-10dT and 11-base single stranded  
15 deoxythymidine (11dT), respectively. In both cases, the data show no peaks from ordered rectangular phase. This result  
16 confirms that end-to-end stacking of short blunt sDNA into long columns is required for forming both 2D ( $L_{\alpha}^{sDNA,2D}$ ) and 3D  
17 columnar phases ( $R_{\alpha}^{sDNA,3D}$ ).

35 For CL-sDNA complexes formed at low mole fraction neutral lipid ( $\Phi_{NL}$ ), stacked sDNA  
36 sandwiched between cationic membranes form columns with a well-defined DNA interaxial spacing in  
37 each layer with no indication of correlations from layer to layer. This 2D columnar phase of stacked  
38 sDNA (labeled  $L_{\alpha}^{sDNA,2D}$ , Fig. 1A, left) is qualitatively similar to the 2D smectic-like organization of  
39 long DNA in cationic liposome-DNA complexes of previous reports (1,45,46). The main difference is  
40 that while the persistence length of DNA ( $\xi_p \approx 500$  Å to 1000 Å) sets the length scale for the 2D smectic  
41 domains of long DNA in the  $L_{\alpha}^C$  phase (i.e. with exponentially decaying in-plane orientational  
42 correlations between domains on scales larger than  $\xi_p$ ), the columns of sDNA are expected to be much  
43 longer than  $\xi_p$  in the  $L_{\alpha}^{sDNA,2D}$  phase. With increasing  $\Phi_{NL}$  ( $0.5 < \Phi_{NL} \leq 0.75$  for 11bp and 24bp sDNA,  
44  
45  
46  
47  
48  
49  
50  
51  
52  
53  
54  
55  
56  
57  
58  
59  
60

1 and  $0.52 < \Phi_{NL} \leq 0.75$  for 48bp sDNA), we observed strong correlations across bilayers through the  
2 onset of a series of new diffraction peaks indicative of long-range order in position and orientation of  
3 sDNA columns. This 3D columnar phase of stacked sDNA, labeled  $R_\alpha^{sDNA,3D}$ , indexes onto a 2D  
4 centered rectangular phase (Fig. 1A, right). We stress that this is the first time a highly organized sDNA  
5 lattice with long-range position and orientation order has been seen in lipid-NA complexes comprised of  
6 fluid membranes.  
7  
8

9 3D columnar phases of long DNA in lipid-DNA complexes have been reported in systems where the  
10 membrane is in the ordered gel phases with chain-frozen lipids (49-51). In the gel phase the very high  
11 membrane bending rigidities ( $\kappa \gg k_B T$ ) effectively suppress thermal undulations giving rise to flat  
12 membranes. Furthermore, because of chain ordering, cationic lipids have limited mobility and provide  
13 little screening of coulombic forces between DNA rods in different layers. Therefore, columnar ordering  
14 occurs due to mutual DNA-DNA repulsions. Our observation of 3D long-range order of sDNA columns  
15 confined between fluid membranes, with lipids in their chain-melted conformation, is highly  
16 unexpected. This is because direct electrostatic DNA-DNA interactions are expected to be short-range  
17 due to screening by liquid-like cationic lipids in the vicinity of the phosphate groups of DNA. Unlike  
18 the case for chain ordered membranes with large  $\kappa$ , the 3D columnar phase of stacked sDNA described  
19 in this paper is strongly enhanced with decreasing  $\kappa$ , which promotes membrane undulations. As  
20 described later, this points to a different origin of ordering where coherent membrane undulations across  
21 layers (Fig. 1A, right) trigger the onset of long-range 3D positional and orientational columnar ordering.  
22  
23

24 The findings of this paper have broader implications in the area of assembly in biological  
25 nanomaterials. Many of the prevailing approaches in hierarchical assembly of nanoscale building blocks  
26 involve either specific interactions, such as H-bonding of complementary nucleic acid base pairs  
27 attached to colloidal nanoparticles (52-55), or nonspecific electrostatic interactions, for example,  
28 between intrinsically disordered protein biopolymers bound to the surface of other structured proteins  
29 (56-58). Here we used the mutual electrostatic coupling of short sDNA rods and flexible membranes as  
30  
31  
32  
33  
34  
35  
36  
37  
38  
39  
40  
41  
42  
43  
44  
45  
46  
47  
48  
49  
50  
51  
52  
53  
54  
55  
56  
57  
58  
59  
60

1 the mechanism for 3D ordering of sDNA. The method may be extended to other nanoparticles of  
2 different shape with a designed-in coupling to membranes; for example, charged peptide rods with built  
3 in end-end hydrophobic interactions, both for structure studies (e.g. fiber diffraction) and as advanced  
4 materials in applications requiring a local high concentration such as biosensing.  
5  
6  
7  
8  
9  
10  
11

## 12 MATERIALS AND METHODS

  
13  
14

15  
16 **DNA Constructs.** All DNA constructs were purchased as single strands from Sigma-Genosys  
17 (Sigma-Aldrich) and delivered as a lyophilized film. All oligos were fully deprotected, leaving  
18 hydroxy 5' ends, and desalting. HPLC was used for oligos  $> 30$  nts (nucleotides). The films were  
19 centrifuged to collect all dried components and then resuspended in 10mM HEPES buffer (pH = 7.0) to  
20  
21  $> 10$  mg/ml. Concentrations were determined by UV-Vis absorption using a ND-1000 UV-Vis  
22 spectrophotometer from NanoDrop Technologies (Thermo Fisher Scientific). Equimolar amounts of  
23 complimentary single strands were mixed and diluted to a final concentration of 10mg/ml. Mixed single  
24 strands were heated in a water bath and held at 90 C for 15 min. The nucleic acids were then slowly  
25 cooled to room temperature to facilitate complete hybridization. Duplexes were run on a 12%  
26 polyacrylamide gel to check for ssDNA contaminants. DNA sequences are listed in Table S1  
27 (Supporting Information). Control sequences of DNA homopolymers, polydeoxyadenylate and  
28 polideoxythymidylate, were purchased at lengths of 11nts, 24nts and 48nts (Sigma-Genosys) and  
29 hybridized or left as single strands.  
30  
31  
32  
33  
34  
35  
36  
37  
38  
39  
40  
41  
42  
43  
44  
45  
46  
47  
48

49 **Lipid Preparation.** 1,2-dioleoyl-3-trimethylammonium-propane (DOTAP) and  
50 1,2-dioleoyl-sn-glycero-3-phosphocholine (DOPC) lipids were purchased from Avanti Polar Lipids  
51 (Alabaster, Alabama) and delivered as lyophilized powders. Liposome solutions were prepared by  
52 dissolving DOTAP and DOPC in trichloromethane to stock concentrations of 30mM respectively. Stock  
53  
54  
55  
56  
57  
58  
59  
60

1 concentrations were mixed at molar ratios (DOTAP:DOPC) of 100:00, 80:20, 40:60 and 30:70 into  
2 glass vials (corresponding to  $\Phi_{NL} = 0, 0.2, 0.6$  and 0.7 respectively). Trichloromethane mixtures of  
3 lipids were then dried under a stream of nitrogen to produce a dried lipid film inside the vial. Dried  
4 films were then placed under vacuum for 24 hours. Films were then rehydrated in ultra pure water to a  
5 final concentration of 30mM and incubated at 37 C. Liposome solutions were sonicated with a  
6 Vibra-Cell (Sonics & Materials, Inc. Newtown, CT) tip sonicator for 10 min and immediately stored at  
7 4 C until use.

19 **Complexes for X-ray.** Complexes for x-ray diffraction were prepared as described previously  
20 (12,14). Briefly, 50  $\mu$ g solutions of DNA or RNA were alloquotted into x-ray quartz capillaries  
21 (Hilgenberg, Malsfeld Germany). Lipid mixtures were added at  $moles_{CL} = \frac{N_{nt}^{NA}}{Z_{CL}} \times \rho_{chg} \times \frac{50\mu g}{MW_{NA}}$  where  
22  $N_{nt}^{NA}$  are the total nucleotides in the DNA or RNA duplex,  $Z_{CL}$  is the cationic lipid headgroup charge (=  
23 +1e for DOTAP) and  $\rho_{chg}$  is the molar charge ratio between CL:NA for the complex. We set  $\rho_{chg} = 1$   
24 such that all complexes tested were isoelectric (each negative charge on DNA is compensated by one  
25 positively charged lipid). After adding appropriate lipid mixtures, capillaries were spun at 1,500 x g for  
26 15 min at 4 C to pellet the condensed aggregate. Capillaries were sealed and stored at 4 C until use.  
27 X-ray diffraction experiments were preformed at Stanford Synchrotron Radiation Lightsource beam line  
28 4-2 using a 1.5 meter flight path with x-ray energy set to 9keV. Data was collected on MX-225  
29 Rayonics (Evanston, IL) CCD detector and radially averaged to produce 1D intensity vs wavevector ( $\mathbf{q}$ )  
30 plots. Before diffraction experiments, samples were either incubated at 37 C for 6 hours or left at 4 C.  
31 Some diffraction experiments were preformed under temperature control using a custom oven with  
32 Minco (Minneapolis, MN) heaters and accuracy  $\pm 0.2$  C. In these samples the temperature was  
33 measured by a thermister, which was in thermal contact with the sample holder.

## 57 RESULTS AND DISCUSSION

## 1 The 2D Columnar Phase of Stacked sDNA (labeled $L_\alpha^{sDNA,2D}$ ) in Cationic Liposome-sDNA

2  
3 **Complexes.** Figure 1B(i) shows synchrotron x-ray scattering data of 11bp sDNA complexed with  
4 DOTAP/DOPC CLs for  $\Phi_{NL} = 0.2$  at the isoelectric point of the complex (i.e. where the number of  
5 negative phosphate groups from sDNA equals the number of cationic charges from DOTAP). The series  
6 of peaks at (00L) ( $L = 1,2,3\dots$ ) results from the multilamellar structure of the complexes with  
7 inter-membrane spacing  $d = 2\pi/q_{001} = 2\pi/(0.104 \text{ \AA}^{-1}) = 60.4 \text{ \AA}$  (Fig. 1A, left). The inter-membrane  
8 distance ( $d$ ) was obtained by fits of the profiles to Lorentzian line-shapes. The inter-membrane distances  
9 are very similar to what is obtained when sDNA is replaced with long (48,502 bp) lambda-phage where  
10  $d (= \delta_m + \delta_w)$  is the thickness of the lipid bilayer membrane ( $\delta_m = 35 \pm 0.5 \text{ \AA}$ ) plus the water layer ( $\delta_w$   
11  $\approx 25 \text{ \AA}$ ) containing a layer of sDNA (sDNA in the hydrated B-conformation has a physical diameter  $\approx$   
12 20  $\text{\AA}$ ) (1,45,46).

13  
14 The broader highly asymmetric peak observed between the (002) and (003) peaks (labeled  $q_{sDNA}$  at  
15 0.239  $\text{\AA}^{-1}$ ) is strikingly similar, both in shape and peak position at the same  $\Phi_{NL}$ , to the diffraction peak  
16 from the 1D lattice of DNA chains (i.e. a 2D smectic) observed previously for lamellar phase CL-DNA  
17 complexes formed with long lambda-phage DNA (45,46). The strong asymmetry, where the lineshape  
18 has a sawtooth shape rising rapidly and falling off slowly after the peak position, is a well-known  
19 signature of powder averaged anisotropic x-ray structure factor of a 1D lattice of rods in  
20 two-dimensions (45). Taken together, the comparison to scattering from long DNA in lamellar  
21 complexes indicates that sDNA molecules, confined between lipid bilayers, are stacked end-to-end  
22 forming long columns with well-defined inter-column spacing (for the data in Fig. 1B(i)  $d_{sDNA} =$   
23  $2\pi/q_{sDNA} = 26.3 \text{ \AA}$  at  $\Phi_{NL} = 0.2$ ). The strong asymmetric lineshape is also a direct indication that the  
24 positional correlations of the 1D lattices across layers is short-range (46). Thus, at  $\Phi_{NL} = 0.2$  cationic  
25 liposome-sDNA complexes form a 2D columnar phase of stacked sDNA ( $L_\alpha^{sDNA,2D}$ ). Interestingly, long  
26 DNA and sDNA complexes differ only in the line widths of the DNA peak, which are inversely  
27 proportional to the square of the line spacing (46).  
28  
29  
30  
31  
32  
33  
34  
35  
36  
37  
38  
39  
40  
41  
42  
43  
44  
45  
46  
47  
48  
49  
50  
51  
52  
53  
54  
55  
56  
57  
58  
59  
60

1 proportional to the coherent domain sizes of the respective 1D lattices and are obtained from the rapidly  
2 rising part of the DNA-DNA lineshape, which is not affected by the powder averaging process in the  
3 lineshape analysis (45,46). Using Lorentzian lineshapes for the structure factor one finds that at  $\Phi_{NL} =$   
4 0.2 the 1D lattice of sDNA columns has a larger coherent domain size  $\approx 460 \text{ \AA}$  ( $\approx 18$  times the unit cell  
5 dimension) by about a factor of four compared to the that for long DNA (1,45,46). This finding is  
6 consistent with the length of the sDNA columns being significantly larger than the persistence length of  
7 DNA, which sets the scale for the domain size of 1D lattices of DNA chains.  
8

9 We should point out that the stacking of blunt sDNA adsorbed on lipid bilayers is not unexpected  
10 because such stacking has been previously observed when sDNA is in aqueous solution (47,48). Blunt  
11 DNAs have an exposed hydrophobic core at each end, an unfavorable situation in the aqueous  
12 environment between bilayer membranes. In B-form DNA, the base pairs are nearly perpendicular to the  
13 longitudinal axis of the DNA strands. Therefore, stacking of blunt DNA ends will put adjacent DNA  
14 molecules in near perfect contact, allowing for greater stability by protecting the hydrophobic core of  
15 bases and creating further  $\pi$ - $\pi$  bonding of the end base's aromatic groups. These non-covalent  
16 interactions would ``glue" the blunt DNA together creating stacks. A similar case has been reported for  
17 the stacking of aromatic dye molecules into columns (59).  
18

19 To further prove the stacking nature of the blunt sDNA, we created complexes with an identical  
20 DNA core (11 bp, perfectly duplexed) but including 10 unpaired deoxythymidine nucleotides to each 3'  
21 end of the duplex (labeled 11DNA-10dT). Diffraction data of 11DNA-10dT complexes at  $\Phi_{NL} = 0.2$  are  
22 shown in Fig. 1B(ii). Interestingly, a very broad peak at  $q_{DNA} = 0.218 \text{ \AA}^{-1}$  can be seen for this sample  
23 ( $\Phi_{NL} = 0.2$ ) indicative of a disordered (isotropic) phase of unstacked duplexes. The addition of 10dT  
24 dangling incompatible single stranded ends prevent end stacking. For comparison, complexes made with  
25 a single-stranded homopolymer of deoxythymidine are included in Figure 1B(iii). These complexes  
26 with single-stranded 11dT DNA show no indication of any correlation peak. The value of  $q_{001}$  for the  
27 ssDNA poly(dT) shifts to larger  $q$  values compared with the dsDNA analog (compare Fig. 1B(iii) to (i))  
28

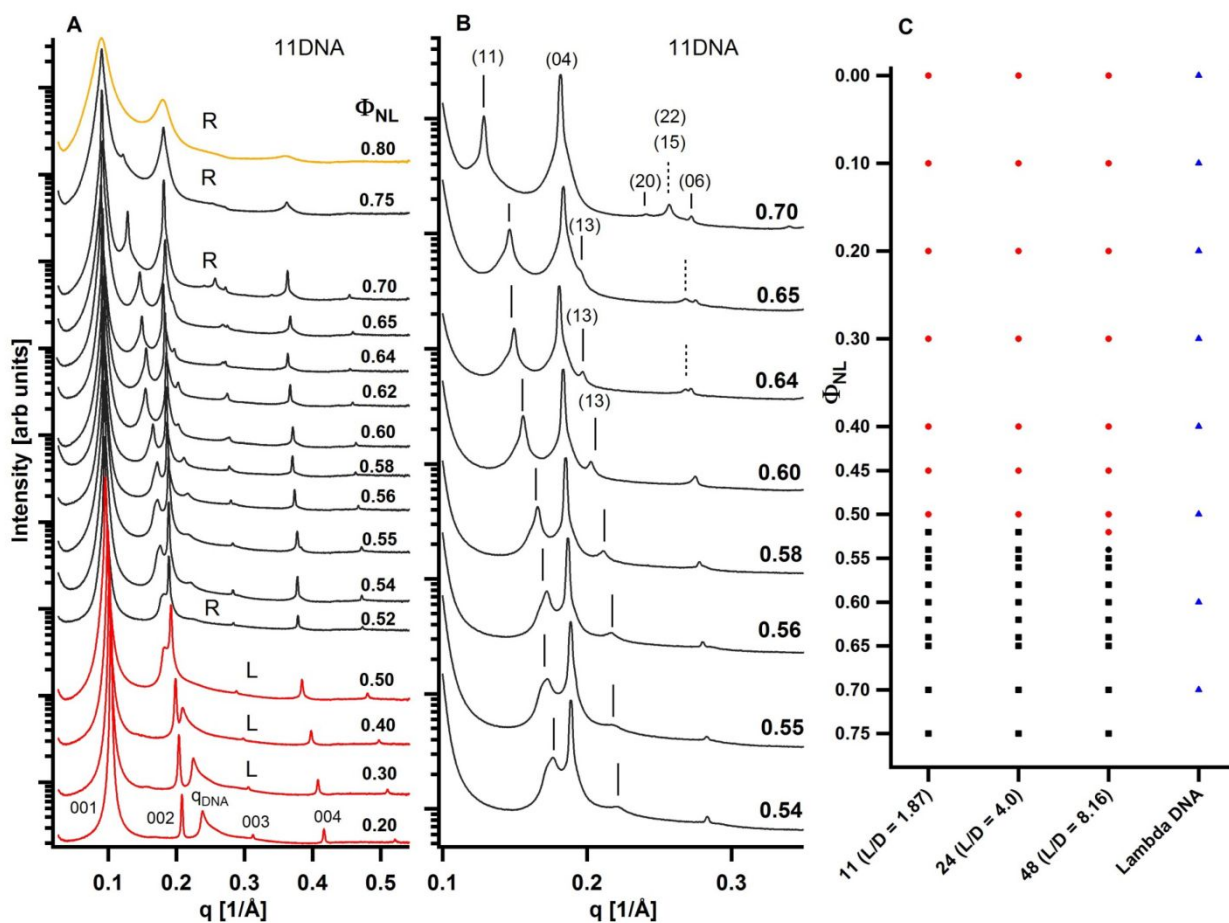
1 indicative of a smaller unit cell normal to the layers. Since lipid composition remains constant between  
2 these samples,  $\delta_m$  must remain fixed and therefore,  $\delta_w$  which contains the 11dT is smaller with the  
3 introduction of ssDNA.  
4  
5  
6  
7  
8  
9

10 **The 3D Columnar Phase of Stacked sDNA (labeled  $R_\alpha^{sDNA,3D}$ ) in Cationic Liposome-sDNA**  
11

12 **Complexes.** At higher neutral lipid compositions ( $\Phi_{NL} > 0.50$  for 11bp and 24bp sDNA and  $\Phi_{NL} > 0.52$   
13 for 48bp sDNA) x-ray scattering data from CL-sDNA complexes shows a phase transition to a new  
14 phase with the onset of new diffraction peaks. Figure 1B(iv) depicts a typical scattering profile in this  
15 new phase for 11bp sDNA at  $\Phi_{NL} = 0.64$  where the sharp peaks, from the diffraction of the sDNA  
16 columns within the lipid bilayers, index to a center rectangular columnar structure with peak positions at  
17 reciprocal lattice vector  $G_{hk} = 2\pi[(h/a)^2 + (k/b)^2]^{1/2}$  with the 2D lattice parameters **a** (= sDNA  
18 intercolumn spacing = 45.9 Å at  $\Phi_{NL} = 0.64$ ) and **b** (= 2\*interlayer spacing  $d = 138.8$  Å at  $\Phi_{NL} = 0.64$ )  
19 as indicated in Figure 1A (right). The observable (h,k) peaks [(02), (11), (04), (13), (15), (06), (08)] all  
20 satisfy the condition that  $h$  plus  $k$  equal an even number as required for a body centered rectangular  
21 lattice. Furthermore, the observation of the 2D center rectangular lattice implies that the sDNA columns  
22 have long-range position and orientation order within the 3D multilayer system; that is, a 3D columnar  
23 phase of stacked sDNA, which we have labeled  $R_\alpha^{sDNA,3D}$  (Fig. 1A, right). To our knowledge, this is the  
24 first time this configuration has been seen in lamellar CL-NA systems with *fluid* membranes (the  
25 subscript “alpha” in the label denotes the liquid state of the membrane due to chain-melted lipids).  
26  
27

28 In figure 1B (v, vi) comparison diffraction data for CL-DNA complexes with 11DNA-10dT and  
29 11-base single stranded deoxythymidine (11dT) are shown, respectively. In both cases, the data show no  
30 peaks from ordered rectangular phase. This result confirms that end-to-end stacking of short blunt  
31 sDNA into long columns is required for forming both 2D ( $L_\alpha^{sDNA,2D}$ ) and 3D columnar phases  
32 ( $R_\alpha^{sDNA,3D}$ ).  
33  
34  
35  
36  
37  
38  
39  
40  
41  
42  
43  
44  
45  
46  
47  
48  
49  
50  
51  
52  
53  
54  
55  
56  
57  
58  
59  
60

1  
2 **Phase Behavior of Stacked sDNA Columns in Cationic Liposome-sDNA Complexes as a Function**  
3 **of Neutral Lipid Composition.** Figure 2A depicts the complete series of synchrotron x-ray scattering  
4 profiles of CL-sDNA complexes for 11bp sDNA as a function of increasing  $\Phi_{NL}$  covering the range  
5 from  $\Phi_{NL} = 0.2$  to  $\Phi_{NL} = 0.8$  (at the isoelectric point of the complex). A plot of a subset of the x-ray  
6 profiles over a smaller q-range for  $\Phi_{NL}$  between 0.54 and 0.70 is shown in figure 2B. This latter figure  
7 more clearly shows the extra diffraction peaks of the  $R_\alpha^{sDNA,3D}$  phase absent in the  $L_\alpha^{sDNA,2D}$  phase; that  
8 is, the (13) peak (solid arrow) for  $\Phi_{NL} = 0.54$  to 0.64, and the (15) peak (dashed arrow) for  $\Phi_{NL} = 0.64$ ,  
9 0.65, and 0.70. The transition from a 2D columnar phase ( $L_\alpha^{sDNA,2D}$ ) to a 3D columnar phase of stacked  
10 sDNA ( $R_\alpha^{sDNA,3D}$ ) occurs between  $\Phi_{NL} = 0.50$  and  $\Phi_{NL} = 0.52$  (where the (13) peak is weak but visible).  
11  
12  
13  
14  
15  
16  
17  
18  
19  
20  
21  
22  
23  
24  
25  
26

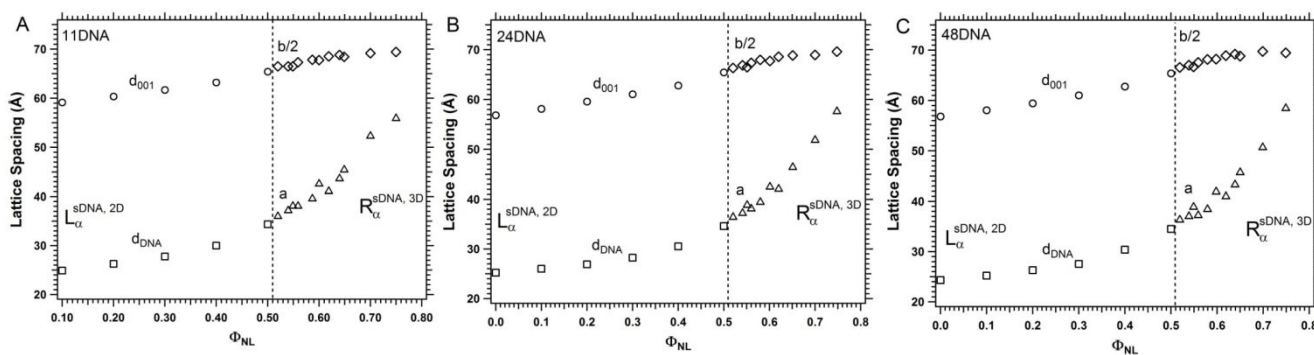


58 **Figure 2.** Phase behavior of stacked sDNA columns in cationic liposome-sDNA complexes as a function of neutral lipid  
59  
60

1 composition. (A) Complete series of synchrotron x-ray scattering profiles of CL-sDNA complexes for 11bp sDNA as a  
2 function of increasing  $\Phi_{NL}$  covering the range from  $\Phi_{NL} = 0.2$  to  $\Phi_{NL} = 0.8$  (at the isoelectric point of the complex). (B) A  
3 plot of a subset of the x-ray profiles over a smaller q-range for  $\Phi_{NL}$  between 0.54 and 0.70, where the onset of rectangular  
4 lattice peaks can be easily seen. (C) Phase diagram, compiled through analysis of x-ray diffraction data, for the  $L_{\alpha}^{sDNA,2D}$   
5 (indicated by black square) and  $R_{\alpha}^{sDNA,3D}$  (indicated by red circle) phases as a function of  $\Phi_{NL}$  for CL-sDNA complexes with  
6 11DNA, 24DNA and 48DNA. All three lengths sDNA behavior similarly. The 4th line shows CL-DNA complexes formed  
7 with long  $\lambda$ -DNA, which remains in the  $L_{\alpha}^C$  phase and do not exhibit a transition to the 3D columnar phase over the entire  
8 range of  $\Phi_{NL}$  between 0 and 0.75.

16  
17  
18  
19 The stability regime for the  $L_{\alpha}^{sDNA,2D}$  and  $R_{\alpha}^{sDNA,3D}$  phases as a function of  $\Phi_{NL}$  for CL-sDNA  
20 complexes with 11DNA, 24DNA and 48DNA is shown in the phase diagram plot in figure 2C. All three  
21 lengths of blunt DNA generally behave the same. For  $\Phi_{NL} \leq 0.50$  for 11DNA and 24DNA and  $\Phi_{NL} \leq$   
22 0.52 for 48DNA, CL-sDNA complexes are in the 2D columnar phase ( $L_{\alpha}^{sDNA,2D}$ ). Here, the diffraction  
23 patterns (Fig. 2A) are strikingly similar to the case of CL-DNA complexes formed with long linear  
24  $\lambda$ -DNA (i.e. the  $L_{\alpha}^C$  phase with DNA sandwiched between cationic membranes (1) where one observes  
25 a highly asymmetric DNA peak significantly broader than the (00L) layering peaks. CL-DNA  
26 complexes with  $\lambda$ -DNA remain in the  $L_{\alpha}^C$  phase. They do not exhibit a transition to the 3D columnar  
27 phase over the entire range of  $\Phi_{NL}$  between 0 and 0.75 beyond which, the  $L_{\alpha}^C$  phase separates with a  
28 lamellar phase with no DNA (45,46) (Fig. 2C, blue triangles). In contrast the 3D columnar phase of  
29 stacked sDNA (black squares) occupies a significant fraction of the phase diagram for larger  $\Phi_{NL}$  ( $0.5 <$   
30  $\Phi_{NL} \leq 0.75$  for 11bp and 24bp sDNA, and  $0.52 < \Phi_{NL} \leq 0.75$  for 48bp sDNA). For even larger  $\Phi_{NL}$  all  
31 diffraction peaks broaden and are indicative of the 3D columnar phase but with smaller domain sizes ( 32  
33 0.80 and 0.85 profiles in Fig. 2A).  
34  
35  
36  
37  
38  
39  
40  
41  
42  
43  
44  
45  
46  
47  
48  
49  
50  
51  
52  
53  
54  
55  
56  
57  
58  
59  
60

We found that annealing the CL-sDNA complexes formed at room temperature by incubation at 37°C for six hours followed by slow cooling to room temperature tended to sharpen the observed diffraction peaks in the  $R_\alpha^{sDNA,3D}$  phase due to annealing of defects resulting in larger coherent domains. This makes the additional higher order peaks associated with the rectangular phase more clearly visible (see supplementary Fig. S1). The incubation period at elevated temperature promotes the dynamics of the short DNAs in order to increase the number of end to end collisions required for stacking. All room temperature samples leading to the phase diagram in figure 2C were subject to temperature annealing. For long lambda-DNA, CL-DNA complexes do not show any significant narrowing of diffraction peaks upon incubation and no evidence of the  $R_\alpha^{sDNA,3D}$  phase is found as a function of varying  $\Phi_{NL}$ .



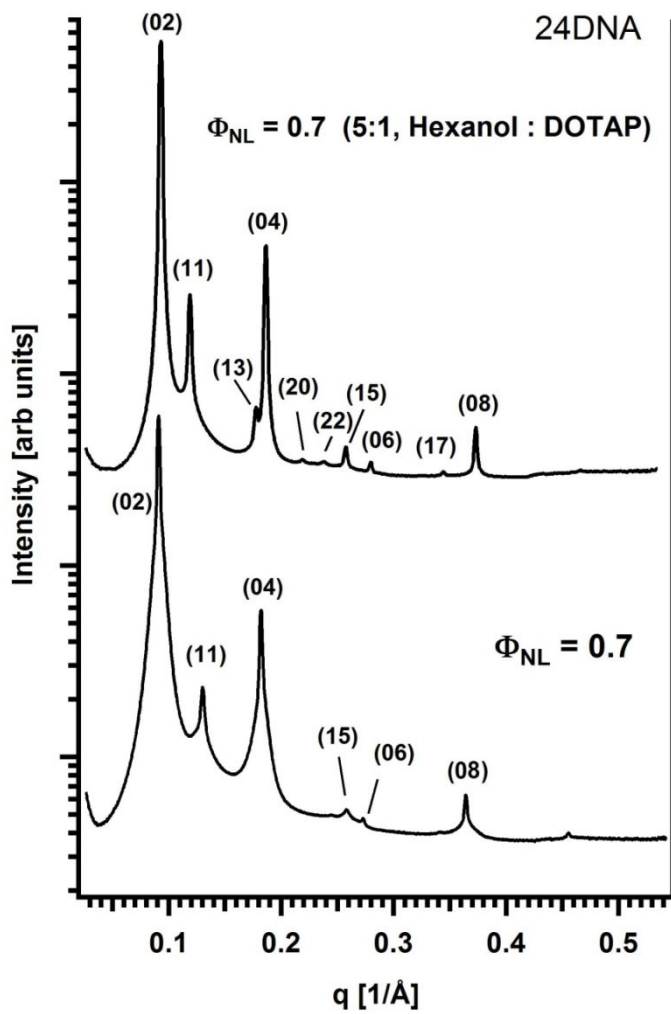
**Figure 3.** Structural parameters derived from synchrotron x-ray scattering data from CL-sDNA complexes for 11bp, 24bp, and 48bp sDNA as a function of  $\Phi_{NL}$  in the  $L_\alpha^{sDNA,2D}$  and  $R_\alpha^{sDNA,3D}$  phases. The vertical dotted lines mark the  $\Phi_{NL}$  point above which  $R_\alpha^{sDNA,3D}$  phase forms. Above the transition, the  $D_{DNA}$  spacing and lipid bilayer spacing  $d_{001}$  in the  $L_\alpha^{sDNA,2D}$  phase become the lattice constants  $a$  and  $b/2$  in the centered rectangular  $R_\alpha^{sDNA,3D}$  phase. (A) Parameters for 11bp sDNA complexes. (B) Parameters for 24bp sDNA complexes. (C) Parameters for 48bp sDNA complexes.

Figure 3 summarizes the structural parameters derived from the synchrotron x-ray scattering data from CL-sDNA complexes for 11bp (A), 24bp (B), and 48bp (C) sDNA as a function of  $\Phi_{NL}$  in the  $L_\alpha^{sDNA,2D}$  and  $R_\alpha^{sDNA,3D}$  phases. This includes the average spacing between sDNA molecules (dsDNA

1 and lattice parameter **a**) and the interlayer spacing (d and **b** = 2\*interlayer spacing) in the  $L_\alpha^{sDNA,2D}$  and  
2  
3  $R_\alpha^{sDNA,3D}$  phases, respectively (see Fig. 1A). We see that  $d_{sDNA}$  and **a** increase with increasing  $\Phi_{NL}$   
4 increases. Thus, the increase in  $\Phi_{NL}$  from 0 to 0.7 leading to a decrease in the average membrane charge  
5 density forces sDNA columns to be further apart. This trend is also observed with CL-DNA containing  
6 long  $\lambda$ -DNA (1). This behavior is due to the fact that within the CL-sDNA complex the average anionic  
7 charge density due to the sDNA has to match the average membrane charge density because of the  
8 requirement of local charge neutrality assuming all counter-ions of the phosphate groups and the  
9 cationic lipid headgroup have been released from the complex into the surrounding solution (1,60).  
10 Figure 3 also shows that the interlayer spacing (d and **b/2**) equal to  $\delta_M$  plus  $\delta_w$  increases with increasing  
11  $\Phi_{NL}$ . This behavior is due to increases both in the membrane bilayer thickness  $\delta_M$  (each DOPC molecule  
12 is  $\approx 4$  Å to 6 Å longer than a DOTAP molecule) and the water layer as  $\Phi_{NL}$  increases because DOPC  
13 has a larger hydration shell compared to DOTAP) (1,20).  
14  
15  
16  
17  
18  
19  
20  
21  
22  
23  
24  
25  
26  
27  
28  
29  
30  
31  
32  
33  
34  
35  
36  
37  
38  
39  
40  
41  
42  
43  
44  
45  
46  
47  
48  
49  
50  
51  
52  
53  
54  
55  
56  
57  
58  
59  
60

**Decrease in the Membrane Bending Rigidity  $\kappa$  Enhances the 3D Columnar Phase in Cationic Liposome-sDNA Complexes ( $R_\alpha^{sDNA,3D}$ ).** To better understand the effect of membrane bending rigidity ( $\kappa$ ) on the stability of the  $R_\alpha^{sDNA,3D}$  phase, we added the membrane soluble co-surfactant hexanol to the lipid mixture prior to complexation with the short DNA for a CL-sDNA complex at  $\Phi_{NL} = 0.7$  well in the  $R_\alpha^{sDNA,3D}$  phase. While co-surfactant molecules, which typically consist of long-chain alcohols (e.g. pentanol, hexanol, heptanol), are not able to stabilize an interface separating hydrophobic and hydrophilic regions, when mixed in with longer chain surfactants they are known to lead to dramatic changes in interface elasticities. Compressional models of surfactant chains (61) show that the bending rigidity ( $\kappa$ ) scales with the membrane thickness  $\kappa \propto \delta_m^P$  with P between 2 and 3. The mixing of co-surfactants with lipids is expected to lead to a thinner membrane and a strong suppression of  $\kappa$

making the membrane highly flexible. Indeed, previous x-ray scattering experiments have shown that the addition of co-surfactants like pentanol, hexanol, and heptanol to lipid membranes of lamellar phases with a mole ratio of between  $\approx 3$  to  $\approx 6$  (i.e. where long chain lipids are effectively surrounded by much shorter chain co-surfactants) leads to a significant decrease of  $\kappa$  from  $\approx 10$  to  $k_B T$  to  $\approx 2-3 k_B T$  (62).

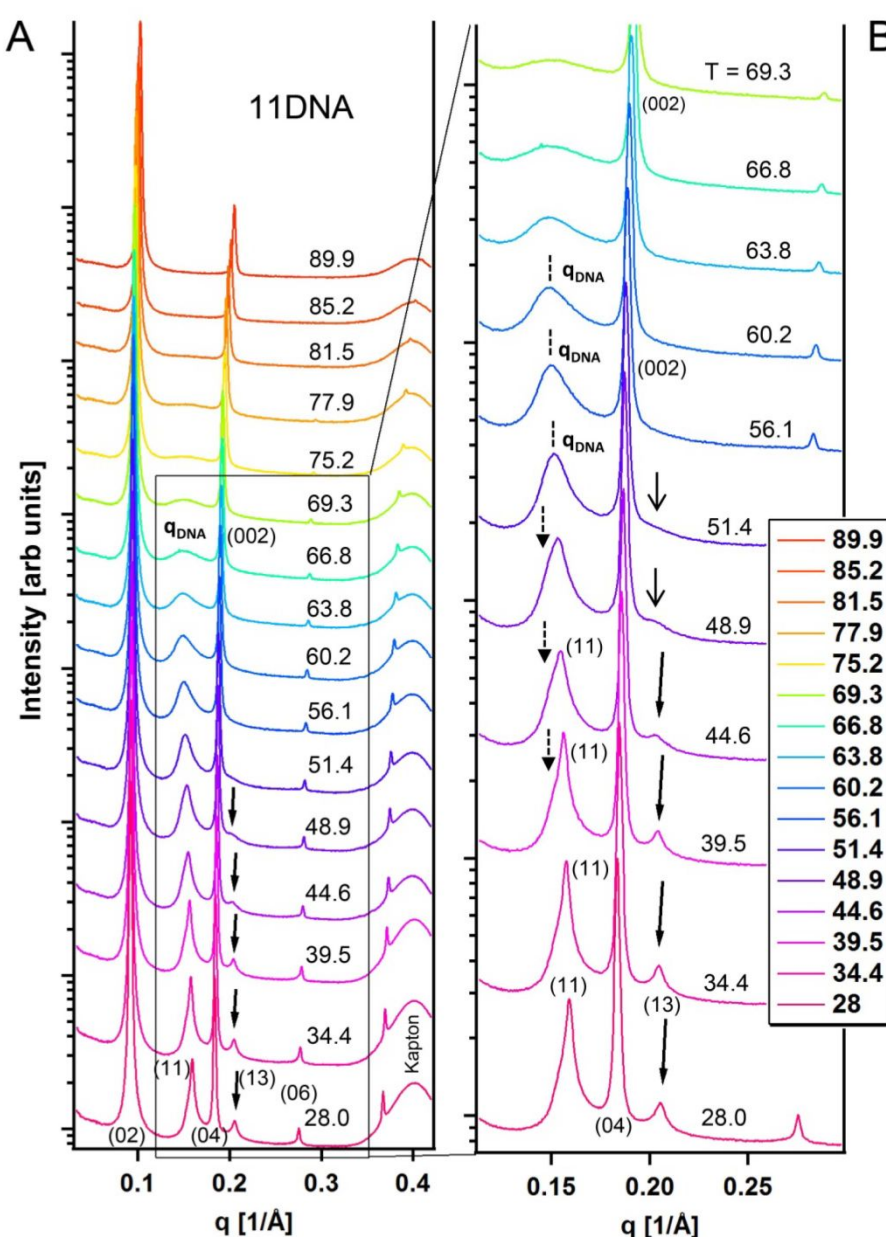


**Figure 4.** Effect of membrane bending rigidity on the stability of the  $R_\alpha^{sDNA,3D}$  phase. Bottom curve shows the x-ray scattering profile from 24bp complex in the  $R_\alpha^{sDNA,3D}$  phase without any co-surfactant, whereas in the top curve, hexanol was added to the sample. The bending rigidity of the membrane is reduced by hexanol, which resulted in significantly sharper and more observable diffraction peaks from the rectangular lattice.

In our studies we added hexanol at a 5:1 molar ratio to total lipid. Figure 4 compares the x-ray scattering profile of CL-sDNA complexes in the  $R_\alpha^{sDNA,3D}$  phase with no added hexanol (bottom) to one with added hexanol (top). One can see immediately that the profiles for complexes with softer membranes display a significant sharpening of the peaks. The narrowing of the diffraction peaks implies larger coherent domains sizes and the presence of longer columns of stacked sDNA) due to softening of the membranes. The larger domain sizes readily leads to observation of additional peaks, in particular,

1 the (20) and (22) of the centered rectangular lattice of sDNA columns, which were buried under the tail  
2 scattering of the wider peaks of the x-ray profiles of complexes with no added hexanol. We also note  
3 that the (13) peak which appears as a shoulder before the (04) peak is clearly visible in complexes  
4 containing hexanol. What is even more remarkable is that whereas the samples with no added hexanol  
5 benefited from incubation at 37 °C for six hours (as discussed in the previous section), no incubation at  
6 elevated temperature was required for the samples with softer membranes and very sharp diffraction  
7 peaks of the  $R_\alpha^{\text{sDNA,3D}}$  phase were immediately apparent with no temperature annealing (Fig. 4 top). As  
8 we discuss below this result is consistent with the fact lowering the rigidity of fluid membranes by  
9 decreasing  $\kappa$  should favor the formation of the  $R_\alpha^{\text{sDNA,3D}}$  phase consisting of coherent membrane  
10 undulations from layer-to-layer.

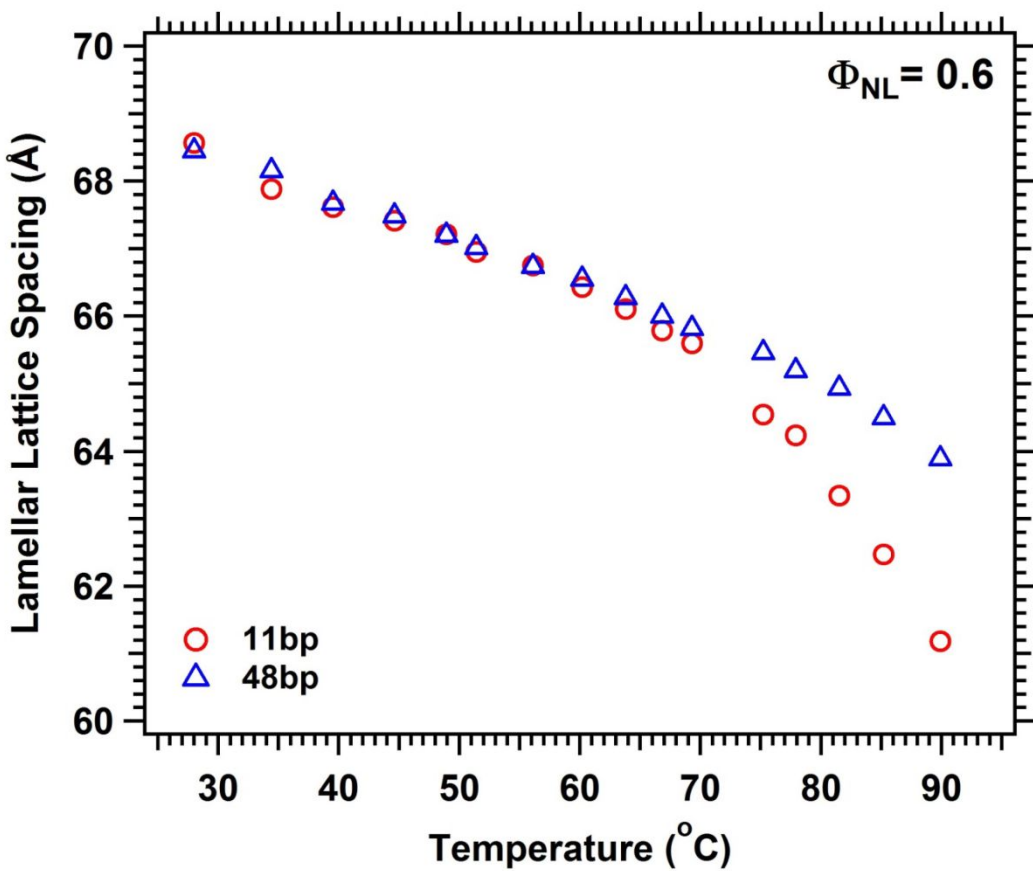
25  
26  
27 **Effect of Temperature on Stacked sDNA Columns in Cationic Liposome-sDNA Complexes.** The  
28 requirement of an incubation step at elevated temperature prompted us to study the CL-sDNA  
29 complexes as a function of temperature. The experiments were performed in-situ by using a temperature  
30 controlled sample chamber (oven). The oven containing the sample typically reached equilibrium in  
31 about 5 minutes, however, each sample was held at the indicated temperature for 15 minutes prior to  
32 x-ray exposure to ensure that the sample had reached equilibrium, which was further confirmed where  
33 subsequent x-ray exposure at a later time did not change the x-ray scattering profile. Scattering profiles  
34 were found to be fully thermally reversible upon slow cooling with peak line widths returning to their  
35 original room temperature values.



**Figure 5.** Effect of temperature on stacked sDNA columns in cationic liposome-sDNA complexes. (A) X-ray scattering data plotted as a function of increasing temperature for CL-sDNA complexes with 11bp DNA in the  $R_\alpha^{sDNA,3D}$  phase at  $\Phi_{NL} = 0.6$ . (B) An expanded view of the x-ray profiles over a smaller q- and temperature range. The (13) peak (see arrows) of the 3D columnar phase (melted in the 2D columnar phase) is used to track structural changes as function of temperature. Between 28 °C to 44.6 °C, where the (13) peaks are sharp (marked by slanted long arrows), the  $R_\alpha^{sDNA,3D}$  phase dominates. At intermediate temperature range  $T = 48.9$  °C and 51.4 °C, the (13) peak is broad and indicate that there is only short range order. At higher temperatures (56.1 °C to  $\approx 69.3$  °C), the (13) peak is completely melted away and the diffraction pattern is indicative of the  $L_\alpha^{sDNA,2D}$  phase. The complete vanishing of the sDNA correlation peak at  $T = 85.2$  °C and 89.9 °C indicates that sDNA are no longer stacked end-to-end and are isotropically distributed between the membrane layers.

1 Figure 5 (A) depicts x-ray scattering data plotted as a function of increasing temperature for  
2 CL-sDNA complexes with 11bp DNA in the  $R_{\alpha}^{sDNA,3D}$  phase at  $\Phi_{NL} = 0.6$ . The right panel (Fig. 5B)  
3 shows an expanded view of the x-ray profiles over a smaller q-range where the (13) peak (see arrows) of  
4 the 3D columnar phase (melted in the 2D columnar phase) is more clearly visible. It is clear from the  
5 data that the  $R_{\alpha}^{sDNA,3D}$  phase is the dominant phase in the lower temperature range ( $T = 28^{\circ}C$  to  $44.6^{\circ}C$ ),  
6 where the (13) diffraction peak indicative of 3D columnar organization remains relatively narrow.  
7 This is compared to a lamellar phase ( $56.1^{\circ}C$  to  $\approx 69.3^{\circ}C$ ), where the (13) peak characteristic of the 3D  
8 columnar phase is melted and where the sharper (11) peak of the  $R_{\alpha}^{sDNA,3D}$  phase is replaced by a  
9 broader  $q_{sDNA}$  indicative of the  $L_{\alpha}^{sDNA,2D}$  phase. On closer inspection one can see that the  $q_{sDNA}$  peak  
10 appears as a shoulder to the (11) peak beginning from  $T = 39.5^{\circ}C$  (dashed arrow) and is the main  
11 broader peak by  $T = 56.1^{\circ}C$  (Fig. 5B). CL-sDNA complexes consisting of 24 bp and 48 bp DNA at  
12  $\Phi_{NL} = 0.6$  show similar temperature dependent behavior with the (13) peak replaced by a broad diffuse  
13 peak by  $T = 48.9^{\circ}C$ . Upon further increases in temperature ( $75.2^{\circ}C$  to  $77.9^{\circ}C$ ) the  $q_{sDNA}$  peak  
14 broadens and vanishes beyond  $85.2^{\circ}C$ .

15  
16 Figure 6 plots the lamellar lattice spacing (membrane bilayer plus a water layer containing the  
17 sDNA columns) as a function of increasing temperature. We see that the spacing decreases smoothly up  
18 to about  $75^{\circ}C$  for both 11 bp sDNA and 48 bp sDNA complexes. This decrease is due to thermal  
19 contraction of the lipid chains. Beyond  $75^{\circ}C$ , we see that both duplexes begin to show a more rapid  
20 decrease in lattice spacing with increasing temperature, with the decrease being much larger for  
21 complexes with the 11 sDNA duplexes. This additional decrease is due to the onset of duplex sDNA  
22 denaturation, which would lead to the observed more rapid rate of decrease in the lamellar lattice  
23 spacing with increasing temperature where the monolayer of duplex sDNA is replaced by a mixture of  
24 denatured single-strand short DNA and double stranded sDNA. Denaturation would also lead to breakup  
25 of the end-to-end interaction and disruption of sDNA columns. This is consistent with the SAXS data of  
26

1  
2  
3  
4  
5 Fig. 5 where the  $q_{sDNA}$  peak is very weak at 77.9 °C and entirely absent at 85.2 °C and 89.9 °C.  
6  
7  
8  
9  
10  
11  
12  
13  
14  
15  
16  
17  
18  
19  
20  
21  
22  
23  
24  
25

32 **Figure 6.** Effects of temperature on lamellar lattice spacing (lipid bilayer plus the water layer containing sDNA) of  
33 CL-sDNA complexes at  $\Phi_{NL} = 0.6$ . The figure shows the spacing as a function of temperature for 11bp and 48bp sDNA. At  
34  $T < 70$  °C the two curves largely overlap, with d-spacing decreasing linearly with increasing T due to thermal contraction of  
35 lipid chains. At  $T > 75$  °C the d-spacing of complexes with 11bp sDNA decreases much faster with temperature indicative of  
36 the onset of denaturation of sDNA (i.e. where the water layer consists of a mixture of single strand and double strand short  
37 DNA). The denaturation effect is much weaker for complexes with 48 bp sDNA.  
38  
39  
40  
41  
42

43  
44  
45  
46 Returning to the profiles at  $T = 48.9$  °C and  $51.4$  °C, we note that the narrow (13) peak is replaced  
47 by a broader diffuse scattering peak (more so for the sample at 48.9 °C than 51.4 °C). This is indicative  
48 of short range positional order between columns from layer to layer absent in the higher temperature  
49 profiles in the 2D columnar phase (56.1 °C to 69.3 °C) with no hint of diffuse scattering near the (13)  
50 peak position. The phase in this intermediate temperature range ( $\approx 48.9$  °C to  $\approx 51.4$  °C) between the  
51  $R_{\alpha}^{sDNA,3D}$  phase and the  $L_{\alpha}^{sDNA,2D}$  phase may indeed be a good candidate for the theoretically predicted  
52  
53  
54  
55  
56  
57  
58  
59  
60

1 sliding columnar phase where the 2D columns in each layer (with finite in-plane compressibility  
2 modulus) readily slide pass each other in neighboring layers, indicative of short range positional order  
3 across layers, but where the columns have 3D long range orientational order (4,5,9).  
4  
5  
6  
7  
8

9 **Origin of Long-Range 3D Positional and Orientational Correlations of the Columns of Stacked**  
10 **sDNA in Cationic Liposome-sDNA Complexes.** A central question related to our findings is the origin  
11 of 3D long-range positional and orientational correlations of the columns of sDNA, given that direct  
12 DNA-DNA electrostatic interactions from layer-to-layer are expected to be short-ranged due to  
13 screening by the cationic lipids diffusing in the liquid phase of the membrane in the vicinity of sDNA  
14 phosphate groups. Our experimental findings are consistent with the theoretical model of Schiessel and  
15 Aranda-Espinoza on layered lipid-DNA complexes. Under equilibrium conditions, coupling of  
16 membrane undulations along the stacking direction promotes coupling of DNA rods in different layers  
17 (63,64). In their model undulations are initiated by the electrostatic wrapping of cationic lipid  
18 membranes around long DNA rods. Furthermore, coherent membrane undulations with wavelength  $\lambda =$   
19  $d_{sDNA}$  (inter-sDNA column spacing, see Fig. 1A, right) are more favorable at large DNA interaxial  
20 spacing because of a significantly lower elastic cost. This is consistent with our experimental finding of  
21 long-range 3D positional and orientational order of sDNA columns at high  $\Phi_{NL}$  (i.e. large  $d_{sDNA}$ ).  
22  
23

24 This may be seen in a calculation of the elastic cost of a sinusoidal membrane undulation along the  
25 x-axis partially wrapped around sDNA columns pointing along the y-axis (Fig. 1A, right). In this model  
26 one may separately consider sinusoidal undulations of the outer and inner monolayers with amplitudes  
27  $h_i$  and  $h_o$ , respectively, where  $h_i = fa$  ( $a$  = radius of sDNA,  $f$  = constant  $< 1$  is a measure of the degree of  
28 membrane wrapping around sDNA columns) and  $h_o = h_i + \delta_m$  (see supplemental section). For each layer  
29 one may write  $h_{o,i}(x) = h_{o,i} \sin(qx)$ , with wavevector  $q = 2\pi/\lambda = 2\pi/d_{sDNA}$  (see Fig. 1A, right). Using the  
30 Helfrich model of curvature elasticity of a fluid membrane (65) we find that the elastic cost per unit area  
31 of a membrane bilayer undulation is  $\propto \kappa h^2 q^4 \propto \kappa h^2/\lambda^4 = \kappa h^2/d_{sDNA}^4$ , where  $h^2 = h_i^2 + h_o^2$  (65). Thus, the  
32  
33  
34  
35  
36  
37  
38  
39  
40  
41  
42  
43  
44  
45  
46  
47  
48  
49  
50  
51  
52  
53  
54  
55  
56  
57  
58  
59  
60

1 rapid decay of elastic cost with increasing inter-sDNA column spacing implies that for large enough  
2  $d_{sDNA}$ , the elastic cost of membrane deformation may be expected to be smaller than the gain in  
3 attractive electrostatic energy due to partial membrane wrapping. This would lead to a stable 3D  
4 columnar phase of stacked sDNA (i.e. the  $R_\alpha^{sDNA,3D}$  phase).

5  
6 Our finding that decreases in the membrane bending rigidity, through addition of the co-surfactant  
7 hexanol to the fluid membranes, strongly enhances the domain size of the  $R_\alpha^{sDNA,3D}$  phase, is further  
8 confirmation of the model where coherent undulation modes giving rise to 3D columnar ordering, is  
9 favored by low  $\kappa$  (63). Thus, long-range position and orientation order of undulations within the  
10 multilayer system; that is, “crystallized undulations” provides a natural mechanism driving the onset of  
11 the 3D columnar phase (Fig. 1A, right).

12  
13 Taken together, our results strongly suggest that the absence of the 3D columnar phase in CL-DNA  
14 complexes with long lambda-phage DNA (1,10,45,46) results from the fact that the DNA chain cannot  
15 be viewed as a model of long rigid rods but rather, on length scales larger than the DNA persistance  
16 length between 50 nm to 100nm, as a meandering flexible rod. Thus, the 3D columnar phase is not  
17 expected to be energetically favorable because the “random” local orientation of long DNA chains is  
18 expected to be uncorrelated between layers. In contrast, CL-sDNA complexes exhibit the 3D columnar  
19 phase precisely because upon stacking they are good models of very long rigid rods and thus the  
20 undulations of one layer may be coherent with other layers over very large membrane areas. Thus,  
21 somewhat counterintuitively, short blunt sDNA, which stacks to produce long rigid rods, provides a  
22 better experimental model of current theoretical models of rigid rods sandwiched between membranes  
23 (63,64,4,5,9) compared to long lambda-phage DNA.

24  
25 Our hypothesis on why the 3D columnar phase is absent in CL-DNA complexes with long  
26 lambda-phage DNA implies that as one increases the length of the blunt sDNA molecule there will be a  
27 length beyond which the new 3D columnar phase reported here will not exist. In fact we expect this to  
28  
29  
30  
31  
32  
33  
34  
35  
36  
37  
38  
39  
40  
41  
42  
43  
44  
45  
46  
47  
48  
49  
50  
51  
52  
53  
54  
55  
56  
57  
58  
59  
60

1 correspond to sDNA molecules that no longer behave as rigid rods but rather exhibit one or two bends  
2 with distances between bends being of order the persistence length of DNA.  
3  
4  
5  
6  
7

## 8 CONCLUSIONS 9

10 3D columnar phases of long DNA confined between membranes in lipid-DNA complexes have been  
11 reported in systems where the flat membranes are in the chain-frozen ordered phase with very high  
12 bending rigidities ( $\kappa \gg k_B T$ ). This is in contrast to our observation of a 3D columnar phase of stacked  
13 short blunt DNA duplexes in flexible fluid multilayer membranes, which, in turn, is further enhanced as  
14 the bending rigidity is lowered by addition of co-surfactant. Chain frozen cationic lipids with no  
15 demixing provide little screening of coulombic forces between DNA rods in different layers and  
16 columnar ordering may occur due to mutual DNA-DNA repulsions. In contrast, our observations are  
17 consistent with coherent macroscopic membrane undulations, electrostatically coupled to sDNA  
18 columns, as the mechanism of inducing long-range position and orientation order of the columns. This  
19 new phase of soft matter may be thought of as a 3D crystal of membrane undulations with repeating unit  
20 cell, consisting of a curved membrane ribbon coupled to a column of sDNA with width equal to the  
21 DNA-DNA interaxial distance and length set by the membrane size. In this sense it is analogous to the  
22 bicontinuous cubic phase with long-range position and orientation order of curved membranes, and the  
23 novel but poorly understood  $P\beta'$  “rippled” phase of multilayer membranes. In the  $P\beta'$  phase, sandwiched  
24 between the commonly observed lamellar  $L\alpha$  (chain melted) and  $L\beta'$  (chain ordered) phases of certain  
25 lecithin-water systems, the membrane modulation unit cell has the symmetry of a 2D monoclinic lattice  
26 (66-68).  
27  
28  
29  
30  
31  
32  
33  
34  
35  
36  
37  
38  
39  
40  
41  
42  
43  
44  
45  
46  
47  
48  
49  
50  
51  
52  
53  
54  
55  
56  
57  
58  
59  
60

## ACKNOWLEDGEMENTS

This work was primarily supported by the US Department of Energy (DOE), Office of Basic Energy Sciences, Division of Materials Sciences and Engineering under award number DE-FG02-06ER46314

(self- and directed assembly in charged biomolecular materials systems). Partial support was further provided by the US National Science Foundation (NSF) under award number DMR-1807327 (membrane phase behavior) and the by the US National Institutes of Health (NIH) under award Number R01GM130769 (efficient packing of small nucleic acids in cationic liposome vectors for delivery applications). C. L. was supported by NSF- DMR 1554435 and NIH- 1DP2EB024377-01. C.E.S. and C.S.M. were supported by NIH RO1AI020611. The research reported here made use of shared experimental facilities of the Materials Research Laboratory at UCSB: an NSF MRSEC (supported by NSF DMR 1720256) and a member of the NSF-supported Materials Research Facilities Network ([www.mrfn.org](http://www.mrfn.org)). The X-ray diffraction work was carried out at the Stanford Synchrotron Radiation Lightsource, a Directorate of SLAC National Accelerator Laboratory and an Office of Science User Facility operated for the US DOE Office of Science by Stanford University.

## REFERENCES

1. Rädler, J. O.; Koltover, I.; Salditt, T.; Safinya, C. R.: Structure of DNA-cationic liposome complexes: DNA intercalation in multilamellar membranes in distinct interhelical packing regimes. *Science* **1997**, *275*, 810-814. DOI: 10.1126/science.275.5301.810.
2. May, S.; Ben-Shaul, A.: DNA-lipid complexes: stability of honeycomb-like and spaghetti-like structures. *Biophys. J.* **1997**, *73*, 2427-2440. DOI: 10.1016/S0006-3495(97)78271-7.
3. Koltover, I.; Salditt, T.; Rädler, J. O.; Safinya, C. R.: An inverted hexagonal phase of cationic liposome-DNA complexes related to DNA release and delivery. *Science* **1998**, *281*, 78-81. DOI: 10.1126/science.281.5373.78.
4. O'Hern, C. S.; Lubensky, T. C.: Sliding Columnar Phase of DNA-Lipid Complexes. *Phys. Rev. Lett.* **1998**, *80*, 4345-4348. DOI: 10.1103/PhysRevLett.80.4345.
5. Golubović, L.; Golubović, M.: Fluctuations of Quasi-Two-Dimensional Smectics Intercalated between Membranes in Multilamellar Phases of DNA-Cationic Lipid Complexes. *Phys. Rev.*

1  
2 *Lett.* **1998**, *80*, 4341-4344. DOI: 10.1103/PhysRevLett.80.4341.

3  
4  
5  
6 6. Harries, D.; May, S.; Gelbart, W. M.; Ben-Shaul, A.: Structure, Stability, and Thermodynamics  
7 of Lamellar DNA-Lipid Complexes. *Biophys. J.* **1998**, *75*, 159-173. DOI:  
8 10.1016/S0006-3495(98)77503-4.

9  
10 7. Bruinsma, R.: Electrostatics of DNA-cationic lipid complexes: isoelectric instability. *Eur. Phys.*  
11 *J. B* **1998**, *4*, 75-88. DOI: 10.1007/s100510050353.

12  
13 8. Bruinsma, R.; Mashl, J.: Long-range electrostatic interaction in DNA-cationic lipid complexes.  
14 *Europhys. Lett.* **1998**, *41*, 165-170. DOI: 10.1209/epl/i1998-00125-0.

15  
16 9. Golubović, L.; Lubensky, T. C.; O'Hern, C. S.: Structural properties of the sliding columnar  
17 phase in layered liquid crystalline systems. *Phys. Rev. E* **2000**, *62*, 1069-1094. DOI:  
18 10.1103/PhysRevE.62.1069.

19  
20 10. Safinya, C. R.: Structures of lipid-DNA complexes: Supramolecular assembly and gene delivery.  
21 *Curr. Opin. Struct. Biol.* **2001**, *11*, 440-448. DOI: 10.1016/S0959-440X(00)00230-X.

22  
23 11. Ewert, K. K.; Evans, H. M.; Zidovska, A.; Bouxsein, N. F.; Ahmad, A.; Safinya, C. R.: A  
24 columnar phase of dendritic lipid-based cationic liposome-DNA complexes for gene delivery:  
25 Hexagonally ordered cylindrical micelles embedded in a DNA honeycomb lattice. *J. Am. Chem.  
26 Soc.* **2006**, *128*, 3998-4006. DOI: 10.1021/ja055907h.

27  
28 12. Bouxsein, N. F.; McAllister, C. S.; Ewert, K. K.; Samuel, C. E.; Safinya, C. R.: Structure and  
29 gene silencing activities of monovalent and pentavalent cationic lipid vectors complexed with  
30 siRNA. *Biochemistry* **2007**, *46*, 4785-4792. DOI: 10.1021/bi062138l.

31  
32 13. Leal, C.; Bouxsein, N. F.; Ewert, K. K.; Safinya, C. R.: Highly Efficient Gene Silencing Activity  
33 of siRNA Embedded in a Nanostructured Gyroid Cubic Lipid Matrix. *J. Am. Chem. Soc.* **2010**,  
34 *132*, 16841-16847. DOI: 10.1021/ja1059763.

35  
36 14. Bouxsein, N. F.; Leal, C. I.; McAllister, C. S.; Ewert, K. K.; Li, Y.; Samuel, C. E.; Safinya, C.  
37 R.: Two-Dimensional Packing of Short DNA with Nonpairing Overhangs in Cationic  
38  
39  
40  
41  
42  
43  
44  
45  
46  
47  
48  
49  
50  
51  
52  
53  
54  
55  
56  
57  
58  
59  
60

1 Liposome–DNA Complexes: From Onsager Nematics to Columnar Nematics with Finite-Length  
2 Columns. *J. Am. Chem. Soc.* **2011**, *133*, 7585-7595. DOI: 10.1021/ja202082c.

3

4 15. Leal, C.; Ewert, K. K.; Bouxsein, N. F.; Shirazi, R. S.; Li, Y.; Safinya, C. R.: Stacking of short  
5 DNA induces the gyroid cubic-to-inverted hexagonal phase transition in lipid-DNA complexes.  
6 *Soft Matter* **2013**, *9*, 795-804. DOI: 10.1039/c2sm27018h.

7

8 16. Kang, M.; Kim, H.; Leal, C.: Self-organization of nucleic acids in lipid constructs. *Curr. Opin.*  
9 *Colloid Interface Sci.* **2016**, *26*, 58-65. DOI: 10.1016/j.cocis.2016.09.006.

10

11 17. Kang, M.; Leal, C.: Soft Nanostructured Films for Actuated Surface-Based siRNA Delivery.  
12 *Adv. Funct. Mater.* **2016**, *26*, 5610-5620. DOI: doi:10.1002/adfm.201600681.

13

14 18. Kim, H.; Sung, J.; Chang, Y.; Alfeche, A.; Leal, C.: Microfluidics Synthesis of Gene Silencing  
15 Cubosomes. *ACS Nano* **2018**, *12*, 9196-9205. DOI: 10.1021/acsnano.8b03770.

16

17 19. Foldvari, M.; Chen, D. W.; Nafissi, N.; Calderon, D.; Narsineni, L.; Rafiee, A.: Non-viral gene  
18 therapy: Gains and challenges of non-invasive administration methods. *J. Controlled Release*  
19 **2016**, *240*, 165-190. DOI: 10.1016/j.jconrel.2015.12.012.

20

21 20. Geinguenaud, F.; Guenin, E.; Lalatonne, Y.; Motte, L.: Vectorization of Nucleic Acids for  
22 Therapeutic Approach: Tutorial Review. *ACS Chem. Biol.* **2016**, *11*, 1180-1191. DOI:  
23 10.1021/acscchembio.5b01053.

24

25 21. Yin, H.; Kauffman, K. J.; Anderson, D. G.: Delivery technologies for genome editing. *Nat. Rev.*  
26 *Drug Discovery* **2017**, *16*, 387-399. DOI: 10.1038/nrd.2016.280.

27

28 22. Safinya, C. R.; Ewert, K. K.; Majzoub, R. N.; Leal, C.: Cationic liposome-nucleic acid  
29 complexes for gene delivery and gene silencing. *New J. Chem.* **2014**, *38*, 5164-5172. DOI:  
30 10.1039/c4nj01314j.

31

32 23. Yin, H.; Kanasty, R. L.; Eltoukhy, A. A.; Vegas, A. J.; Dorkin, J. R.; Anderson, D. G.: Non-viral  
33 vectors for gene-based therapy. *Nat. Rev. Genet.* **2014**, *15*, 541-555. DOI: 10.1038/nrg3763.

34

35 24. Wang, Y.; Miao, L.; Satterlee, A.; Huang, L.: Delivery of oligonucleotides with lipid  
36

1 nanoparticles. *Adv. Drug Delivery Rev.* **2015**, *87*, 68-80. DOI: 10.1016/j.addr.2015.02.007.

2 25. Ewert, K. K.; Kotamraju, V. R.; Majzoub, R. N.; Steffes, V. M.; Wonder, E. A.; Teesalu, T.;  
3 Ruoslahti, E.; Safinya, C. R.: Synthesis of linear and cyclic peptide-PEG-lipids for stabilization  
4 and targeting of cationic liposome-DNA complexes. *Bioorg. Med. Chem. Lett.* **2016**, *26*,  
5 1618-1623. DOI: 10.1016/j.bmcl.2016.01.079.

6 12. Majzoub, R. N.; Ewert, K. K.; Safinya, C. R.: Cationic liposome-nucleic acid nanoparticle  
7 assemblies with applications in gene delivery and gene silencing. *Philos. Trans. R. Soc., A* **2016**,  
8 374. DOI: 10.1098/rsta.2015.0129.

9 27. Guo, X.; Huang, L.: Recent Advances in Nonviral Vectors for Gene Delivery. *Acc. Chem. Res.*  
10 **2012**, *45*, 971-979. DOI: 10.1021/ar200151m.

11 28. Safinya, C. R.; Ewert, K. K.: Materials chemistry: Liposomes derived from molecular vases.  
12 *Nature* **2012**, *489*, 372-374.

13 29. Bielke, W.; Erbacher, C., Eds.: *Nucleic Acid Transfection*. Springer: Berlin, **2010**.

14 30. Ewert, K.; Zidovska, A.; Ahmad, A.; Bouxsein, N.; Evans, H.; McAllister, C.; Samuel, C.;  
15 Safinya, C.: Cationic Liposome-Nucleic Acid Complexes for Gene Delivery and Silencing:  
16 Pathways and Mechanisms for Plasmid DNA and siRNA. In *Nucleic Acid Transfection*, Bielke,  
17 W.; Erbacher, C., Eds. Springer: Berlin, **2010**; pp. 191-226. DOI: 10.1007/128\_2010\_70.

18 31. Huang, L.; Hung, M. C.; Wagner, E., Eds.: *Non-Viral Vectors for Gene Therapy*. 2nd ed.;  
19 Elsevier Academic Press: San Diego, **2005**.

20 32. Ewert, K.; Ahmad, A.; Evans, H.; Safinya, C.: Cationic lipid-DNA complexes for non-viral gene  
21 therapy: relating supramolecular structures to cellular pathways. *Expert Opin. Biol. Ther.* **2005**,  
22 5, 33-53. DOI: 10.1517/14712598.5.1.33.

23 33. Young, S. W. S.; Stenzel, M.; Jia-Lin, Y.: Nanoparticle-siRNA: A potential cancer therapy?  
24 *Crit. Rev. Oncol.* **2016**, *98*, 159-169. DOI: 10.1016/j.critrevonc.2015.10.015.

25 34. Ozcan, G.; Ozpolat, B.; Coleman, R. L.; Sood, A. K.; Lopez-Berestein, G.: Preclinical and

1 clinical development of siRNA-based therapeutics. *Adv. Drug Delivery Rev.* **2015**, *87*, 108-119.

2 DOI: 10.1016/j.addr.2015.01.007.

3

4 35. Rupaimoole, R.; Slack, F. J.: MicroRNA therapeutics: towards a new era for the management of

5 cancer and other diseases. *Nat. Rev. Drug Discovery* **2017**, *16*, 203-222. DOI:

6 10.1038/nrd.2016.246.

7

8 36. Guan, S.; Rosenecker, J.: Nanotechnologies in delivery of mRNA therapeutics using nonviral

9 vector-based delivery systems. *Gene Ther.* **2017**, *24*, 133-143. DOI: 10.1038/gt.2017.5.

10

11 37. Wan, C.; Allen, T. M.; Cullis, P. R.: Lipid nanoparticle delivery systems for siRNA-based

12 therapeutics. *Drug Delivery Transl. Res.* **2014**, *4*, 74-83. DOI: 10.1007/s13346-013-0161-z.

13

14 38. Gindy, M. E.; Leone, A. M.; Cunningham, J. J.: Challenges in the pharmaceutical development

15 of lipid-based short interfering ribonucleic acid therapeutics. *Expert Opin. Drug Delivery* **2012**,

16 9, 171-182. DOI: 10.1517/17425247.2012.642363.

17

18 39. Gindy, M. E.; DiFelice, K.; Kumar, V.; Prud'homme, R. K.; Celano, R.; Haas, R. M.; Smith, J.

19 S.; Boardman, D.: Mechanism of Macromolecular Structure Evolution in Self-Assembled Lipid

20 Nanoparticles for siRNA Delivery. *Langmuir* **2014**, *30*, 4613-4622. DOI: 10.1021/la500630h.

21

22 40. Pecot, C. V.; Calin, G. A.; Coleman, R. L.; Lopez-Berestein, G.; Sood, A. K.: RNA interference

23 in the clinic: challenges and future directions. *Nat. Rev. Cancer* **2011**, *11*, 59-67.

24

25 41. Lares, M. R.; Rossi, J. J.; Ouellet, D. L.: RNAi and small interfering RNAs in human disease

26 therapeutic applications. *Trends Biotechnol.* **2010**, *28*, 570-579. DOI:

27 10.1016/j.tibtech.2010.07.009.

28

29 42. Leal, C.; Ewert, K. K.; Shirazi, R. S.; Bouxsein, N. F.; Safinya, C. R.: Nanoglycoids

30 Incorporating Multivalent Lipids: Enhanced Membrane Charge Density and Pore Forming

31 Ability for Gene Silencing. *Langmuir* **2011**, *27*, 7691-7697. DOI: 10.1021/la200679x.

32

33 43. Gene Therapy Clinical Trials Worldwide. The Journal of Gene Medicine clinical trial site.

34 <http://www.wiley.com/legacy/wileychi/genmed/clinical/> (accessed August, 2019).

35

36

37

38

39

40

41

42

43

44

45

46

47

48

49

50

51

52

53

54

55

56

57

58

59

60

1 44. Ginn, S. L.; Amaya, A. K.; Alexander, I. E.; Edelstein, M. L.; Abedi, M. R.: Gene therapy  
2 clinical trials worldwide to 2017 – an update. *J. Gene Med.* **2018**, 2018;20:e3015. <https://doi.org/10.1002/jgm.3015>

3 45. Salditt, T.; Koltover, I.; Rädler, J. O.; Safinya, C. R.: Two-dimensional smectic ordering of  
4 linear DNA chains in self-assembled DNA-cationic liposome mixtures. *Phys. Rev. Lett.* **1997**,  
5 79, 2582-2585.

6 46. Salditt, T.; Koltover, I.; Rädler, J. O.; Safinya, C. R.: Self-assembled DNA-cationic-lipid  
7 complexes: Two-dimensional smectic ordering, correlations, and interactions. *Phys. Rev. E*  
8 **1998**, 58, 889-904.

9 47. Nakata, M.; Zanchetta, G.; Chapman, B. D.; Jones, C. D.; Cross, J. O.; Pindak, R.; Bellini, T.;  
10 Clark, N. A.: End-to-End Stacking and Liquid Crystal Condensation of 6– to 20–Base Pair DNA  
11 Duplexes. *Science* **2007**, 318, 1276-1279. DOI: 10.1126/science.1143826.

12 48. Zanchetta, G.; Bellini, T.; Nakata, M.; Clark, N. A.: Physical Polymerization and Liquid  
13 Crystallization of RNA Oligomers. *J. Am. Chem. Soc.* **2008**, 130, 12864-12865. DOI:  
14 10.1021/ja804718c.

15 49. Artzner, F.; Zantl, R.; Rapp, G.; Rädler, J. O.: Observation of a Rectangular Columnar Phase in  
16 Condensed Lamellar Cationic Lipid-DNA Complexes. *Phys. Rev. Lett.* **1998**, 81, 5015-5018.  
17 DOI: 10.1103/PhysRevLett.81.5015.

18 50. Koynova, R.; MacDonald, R. C.: Columnar DNA Superlattices in Lamellar  
19 o-Ethylphosphatidylcholine Lipoplexes: Mechanism of the Gel-Liquid Crystalline Lipid Phase  
20 Transition. *Nano Lett.* **2004**, 4, 1475-1479. DOI: 10.1021/nl049191k.

21 51. McManus, J. J.; Rädler, J. O.; Dawson, K. A.: Observation of a Rectangular Columnar Phase in  
22 a DNA–Calcium–Zwitterionic Lipid Complex. *J. Am. Chem. Soc.* **2004**, 126, 15966-15967.  
23 DOI: 10.1021/ja046105+.

24 52. Mirkin, C. A.; Letsinger, R. L.; Mucic, R. C.; Storhoff, J. J.: A DNA-based method for rationally  
25

1 assembling nanoparticles into macroscopic materials. *Nature* **1996**, *382*, 607-609.  
2  
3  
4  
5  
6  
7  
8  
9

10 53. Elghanian, R.; Storhoff, J. J.; Mucic, R. C.; Letsinger, R. L.; Mirkin, C. A.: Selective  
11 Colorimetric Detection of Polynucleotides Based on the Distance-Dependent Optical Properties  
12 of Gold Nanoparticles. *Science* **1997**, *277*, 1078-1081. DOI: 10.1126/science.277.5329.1078.  
13  
14 54. Nykypanchuk, D.; Maye, M. M.; van der Lelie, D.; Gang, O.: DNA-guided crystallization of  
15 colloidal nanoparticles. *Nature* **2008**, *451*, 549-552. DOI: 10.1038/nature06560.  
16  
17 55. Maye, M. M.; Nykypanchuk, D.; van der Lelie, D.; Gang, O.: A Simple Method for Kinetic  
18 Control of DNA-Induced Nanoparticle Assembly. *J. Am. Chem. Soc.* **2006**, *128*, 14020-14021.  
19 DOI: 10.1021/ja0654229.  
20  
21 56. Chung, P. J.; Song, C.; Deek, J.; Miller, H. P.; Li, Y.; Choi, M. C.; Wilson, L.; Feinstein, S. C.;  
22 Safinya, C. R.: Tau mediates microtubule bundle architectures mimicking fascicles of  
23 microtubules found in the axon initial segment. *Nat. Commun.* **2016**, *7*, 12278. DOI:  
24 10.1038/ncomms12278.  
25  
26 57. Deek, J.; Chung, P. J.; Kayser, J.; Bausch, A. R.; Safinya, C. R.: Neurofilament sidearms  
27 modulate parallel and crossed-filament orientations inducing nematic to isotropic and re-entrant  
28 birefringent hydrogels. *Nat. Commun.* **2013**, *4*, 2224. DOI: 10.1038/ncomms3224.  
29  
30  
31 58. Beck, R.; Deek, J.; Choi, M. C.; Ikawa, T.; Watanabe, O.; Frey, E.; Pincus, P.; Safinya, C. R.:  
32 Unconventional Salt Trend from Soft to Stiff in Single Neurofilament Biopolymers. *Langmuir*  
33  
34 **2010**, *26*, 18595-18599. DOI: 10.1021/la103655x.  
35  
36  
37 59. Horowitz, V. R.; Janowitz, L. A.; Modic, A. L.; Heiney, P. A.; Collings, P. J.: Aggregation  
38 behavior and chromonic liquid crystal properties of an anionic monoazo dye. *Phys. Rev. E* **2005**,  
39  
40 72, 041710. DOI: 10.1103/PhysRevE.72.041710.  
41  
42  
43 60. Koltover, I.; Salditt, T.; Safinya, C. R.: Phase diagram, stability, and overcharging of lamellar  
44 cationic lipid- DNA self-assembled complexes. *Biophys. J.* **1999**, *77*, 915-924. DOI:  
45 10.1016/S0006-3495(99)76942-0.  
46  
47  
48  
49  
50  
51  
52  
53  
54  
55  
56  
57  
58  
59  
60

1 61. Szleifer, I.; Kramer, D.; Ben-Shaul, A.; Roux, D.; Gelbart, W. M.: Curvature Elasticity of Pure  
2 and Mixed Surfactant Films. *Phys. Rev. Lett.* **1988**, *60*, 1966-1969. DOI:  
3 10.1103/PhysRevLett.60.1966.

4 62. Safinya, C. R.; Sirota, E. B.; Roux, D.; Smith, G. S.: Universality in interacting membranes: The  
5 effect of cosurfactants on the interfacial rigidity. *Phys. Rev. Lett.* **1989**, *62*, 1134-1137.

6 63. Schiessel, H.; Aranda-Espinoza, H.: Electrostatically induced undulations of lamellar DNA-lipid  
7 complexes. *Eur. Phys. J. E* **2001**, *5*, 499-506. DOI: 10.1007/s101890170057.

8 64. Schiessel, H.: Bending of charged flexible membranes due to the presence of macroions. *Eur.*  
9 *Phys. J. B* **1998**, *6*, 373-380. DOI: 10.1007/s100510050563.

10 65. Helfrich, W.: Steric Interaction of Fluid Membranes in Multilayer Systems. *Z. Naturforsch. A*  
11 **1978**, *33*, 305-315. DOI: 10.1515/zna-1978-0308.

12 66. Wack, D. C.; Webb, W. W.: Synchrotron x-ray study of the modulated lamellar phase  $P_{\beta'}$  in the  
13 lecithin-water system. *Phys. Rev. A* **1989**, *40*, 2712-2730. DOI: 10.1103/PhysRevA.40.2712.

14 67. Zasadzinski, J.; Schneir, J.; Gurley, J.; Elings, V.; Hansma, P.: Scanning tunneling microscopy  
15 of freeze-fracture replicas of biomembranes. *Science* **1988**, *239*, 1013-1015. DOI:  
16 10.1126/science.3344420.

17 68. Sirota, E. B.; Smith, G. S.; Safinya, C. R.; Plano, R. J.; Clark, N. A.: X-ray scattering studies of  
18 aligned, stacked surfactant membranes. *Science* **1988**, *242*, 1406-1409.

19  
20  
21  
22  
23  
24  
25  
26  
27  
28  
29  
30  
31  
32  
33  
34  
35  
36  
37  
38  
39  
40  
41  
42  
43  
44  
45  
46  
47  
48  
49  
50  
51  
52  
53  
54  
55  
56  
57  
58  
59  
60